nature physics

Article

https://doi.org/10.1038/s41567-023-02338-3

Observation of fixed lines induced by a nonlinear resonance in the CERN Super Proton Synchrotron

Received: 12 December 2022

Accepted: 14 November 2023

Published online: 20 March 2024

Check for updates

H. Bartosik [1] ✉, G. Franchetti [2,3,4] ✉ & F. Schmidt [1] ✉

The motion of systems with linear restoring forces and recurring nonlinear perturbations is of central importance in physics. When a system's natural oscillation frequencies and the frequency of the nonlinear restoring forces satisfy certain algebraic relations, the dynamics become resonant. In accelerator physics, an understanding of resonances and nonlinear dynamics is crucial for avoiding the loss of beam particles. Here we confirm the theoretical prediction of the dynamics for a single two-dimensional coupled resonance by observing so-called fixed lines. Specifically, we use the CERN Super Proton Synchrotron to measure the position of a particle beam at discrete locations around the accelerator. These measurements allow us to construct the Poincaré surface of section, which captures the main features of the dynamics in a periodic system. In our setting, any resonant particle passing through the Poincaré surface of section lies on a curve embedded in a four-dimensional phase space, the fixed line. These findings are relevant for mitigating beam degradation and thus for achieving high-intensity and high-brightness beams, as required for both current and future accelerator projects.

The complexity of resonant dynamics depends on the number of degrees of freedom of the problem. A pendulum has one degree of freedom[1], whereas a chain of N masses bounded by springs forming a Fermi–Pasta–Ulam system[2] has N degrees of freedom. The main features of the dynamics in a periodic system are captured by the Poincaré surface of section, an approach invented by Henri Poincaré to study the dynamics of nonlinear systems[3]. The resonant dynamics for a one-dimensional (1D) periodic system is characterized by special orbits in the Poincaré surface of section. These are fixed points, islands and separatrices, as shown at the top left of Fig. 1a. The next level of complexity is a periodic system with two degrees of freedom. In this case, the orbits in the Poincaré surface of section expand into a four-dimensional phase space, the topology of which may elude our geometric intuition. In the simplest case, the two degrees of freedom (Fig. 1a) are decoupled, and the 'mixed' coordinates (q_1, q_2) and (p_1, p_2) exhibit the characteristic rectangular shape[4], as shown in the bottom row of Fig. 1a (for experimental evidence, see ref. 5). Instead, for resonant dynamics created by a nonlinear coupling force, the mixed coordinates may exhibit a specific correlation, as shown, for example, in Fig. 1b. This feature can be quite surprising, as each (q, p) plane per degree of freedom seems unaffected, with information about the resonant dynamics being only in the mixed planes. Note that the four diagrams in Fig. 1b show that the collection of all the red points lies on a four-dimensional closed curve, which we call a 'fixed line'[6], as any resonant particle at any passage through the Poincaré surface of section is located somewhere on this curve[7].

Charged particles in circular accelerators have two degrees of freedom in the transverse plane. Nonlinear forces due to magnet imperfections may drive resonance structures in phase space, which has always been a subject of practical concern for (1) avoiding resonances[8–11]

[1]CERN, European Organisation for Nuclear Research, Geneva, Switzerland. [2]GSI Helmholtzzentrum für Schwerionenforschung GmbH, Darmstadt, Germany. [3]Goethe University Frankfurt, Frankfurt am Main, Germany. [4]Helmholtz Forschungsakademie Hessen für FAIR (HFHF), GSI Helmholtzzentrum für Schwerionenforschung, Campus Frankfurt, Frankfurt am Main, Germany. ✉e-mail: hannes.bartosik@cern.ch; g.franchetti@gsi.de; frank.schmidt@cern.ch

https://doi.org/10.1038/s41567-023-02338-3

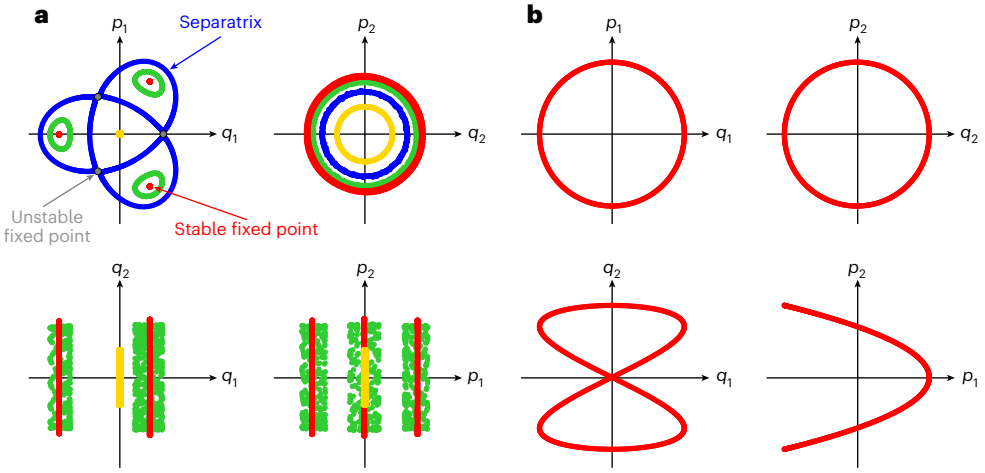

Fig. 1 | Effect of the coupled resonance for a system with two degrees of freedom. a, Poincaré surface of section for a 1D resonance acting in a system with two degrees of freedom. The top left diagram shows the main features of the orbits for a 1D resonance with canonical coordinates (q_1, p_1). The blue curves are the orbit of the separatrix, which crosses the unstable fixed points; The red dots indicate the stable fixed points. The green curves represent orbits inside the resonance islands. The yellow dot is an orbit passing through the origin of the phase space plane of coordinates 1. The top right diagram shows the non-resonant orbits for the second degree of freedom, which are now circles. The colours correspond to the same four test particles as in the top left diagram. The bottom row shows the resonant orbits in the 'mixed' planes (q_1, q_2) and (p_1, p_2). The characteristic rectangular shape of the areas covered by the orbits is a signature of decoupling (green markers). **b**, Poincaré surfaces of section in a system with two degrees of freedom subject to a 2D nonlinear resonance. The effect of the resonance is visible only in the mixed coordinate diagrams[7].

and (2) keeping the dynamic aperture (DA)[12] large enough to ensure sufficient beam lifetime[13–15]. A prominent example of the impact of nonlinearities in accelerators is the Large Hadron Collider (LHC)[16], which was commissioned at CERN in 2008. The LHC is constructed with superconducting magnets that inherently generate unwanted nonlinear field components. Based on the experience with previous superconducting colliders, the LHC had to be designed with a DA larger by a factor of two than the target value to ensure stable operation with a safety margin. However, after a systematic effort on the measurement and modelling of the LHC magnet-to-magnet nonlinearities at CERN, a beam experiment in 2012 demonstrated that the two-dimensional (2D) DA of the LHC agreed within 10% with the predictions of the simulations[17]. Further confirmations of the correlation of the real beam lifetime to the DA were reported later[18].

When designing future high-energy colliders[19–21], optimizing the superconducting magnets will require a similar systematic effort as was done for the LHC, including the study of 2D resonances, as in this study. If we can predict the DA with 10% precision, the additional safety margin of a factor of two may not be required, and thus, a considerable cost saving can be achieved.

For lower-energy accelerators, nonlinear resonances are of concern for high-intensity and high-brightness beams, as for the SIS100 in the Facility for Antiproton and Ion Research[22,23] at GSI, and for the operation of the accelerator chain at CERN after the LHC injectors upgrade[24]. Studies performed over the last 20 years on 1D resonances have shown that space-charge-induced resonance crossing is a prominent mechanism behind halo formation and associated particle loss for high-intensity bunches[25,26]. Recent studies have suggested that fixed lines cause the formation of asymmetric halos[27]. However, the existence of fixed lines has never been proven experimentally, confining any discussion merely to computer simulations or analytical methods. This situation is unsatisfactory, especially because fixed lines are invoked as part of the complex mechanism for periodic resonance crossing, thus motivating the experimental verification of their existence.

The dynamical coordinates of a particle in the transverse plane are (x, y) and the conjugate momenta are p_x and p_y. To these coordinates we associate the horizontal and vertical phase advances ϕ_x and ϕ_y, respectively[28]. The oscillation frequencies are expressed in terms of the number of oscillations per turn, Q_x and Q_y, which are also called the tunes or the working point in the accelerator community. We consider the case of one or more normal sextupole magnets of integrated strength K_2 inserted in an otherwise linear accelerator structure. The resonance condition $Q_x + 2Q_y = N$ combines the phase advances of the

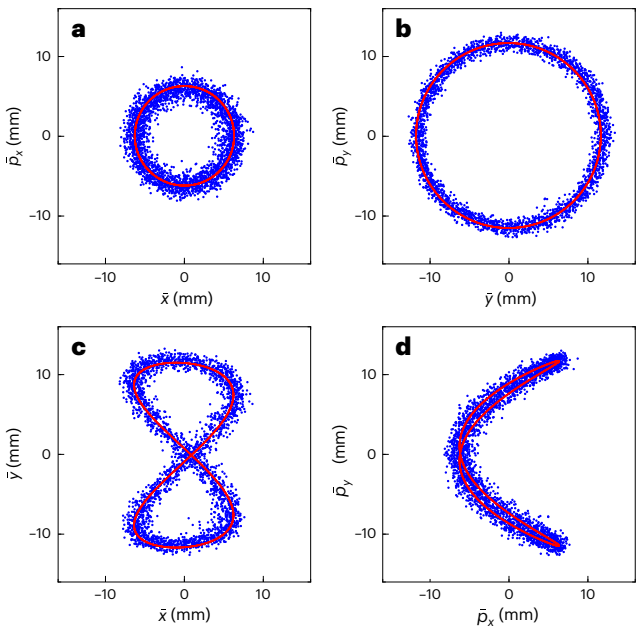

Fig. 2 | Measured Poincaré surface of section. a–d, Four projections of a Poincaré surface of section. The blue markers are the scaled beam coordinates obtained experimentally from 3,000 passages through the selected longitudinal observation point. **a**, Projection of horizontal position and momentum expressed in scaled Courant–Snyder coordinates. The circular shape shows that the amplitude $\bar{a}_x$ is constant. **b**, Projection in the $(\bar{y}, \bar{p}_y)$ plane. The orbit is circular showing that $\bar{a}_y$ is constant. **c**,**d**, In the mixed coordinates, $(\bar{x}, \bar{y})$ (**c**) and $(\bar{p}_x, \bar{p}_y)$ (**d**), the motion of the beam follows a Lissajous curve. The spread of the markers yields direct information on the random error created by the four BPMs, with standard deviations $\sigma_{\mathrm{BPM},x} \approx 0.66$ mm and $\sigma_{\mathrm{BPM},y} \approx 0.5$ mm. The red line is the best fit of equation (1) to the experimental data, which confirms that the topology is consistent with that of a fixed line.

https://doi.org/10.1038/s41567-023-02338-3

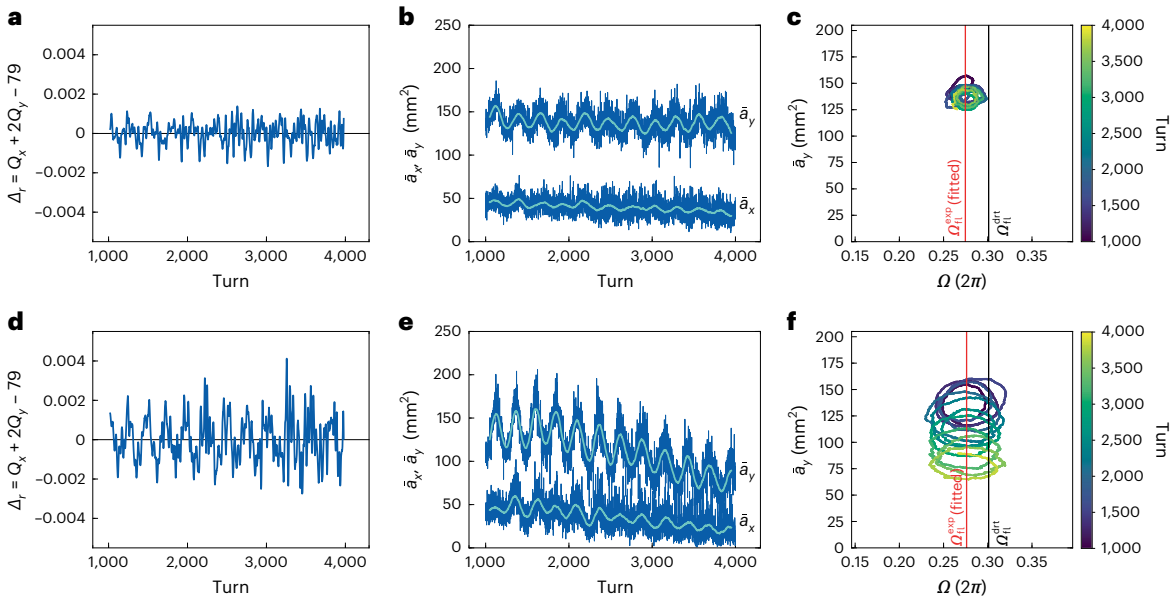

Fig. 3 | Finding fixed lines and their properties. a–**c**, A case with the stable features of Fig. 2. **d**–**f**, A case where the machine conditions (in particular the machine tunes) are subject to unwanted drift. **a**, Evolution of the distance from the resonance calculated using the measured beam tunes, Q_x and Q_y. The harmonic number of the resonance is 79. **b**, Evolution of $\bar{a}_x$ and $\bar{a}_y$, the scaled Courant–Snyder forms (dark blue), and their corresponding moving averages (light blue; Methods). **c**, $\bar{a}_y$ versus Ω diagram, where $\Omega = \phi_x + 2\phi_y$. This beam revolves over 3,000 turns around a 'fixed point'. The red vertical line is the fitted value of Ω. The black vertical line is the value of Ω found from the driving term calculations. **d**, Evolution of the distance from the resonance calculated using the measured beam tunes. There are larger oscillations over time. **e**, Evolution of $\bar{a}_x$ and $\bar{a}_y$. The variation is larger but the variables are still correlated. **f**, $\bar{a}_y$ versus Ω diagram. The meaning of the red and black vertical lines is the same as in **c**. The quantity $\bar{a}_y$ spans over a large range, whereas Ω keeps oscillating around one specific Ω_{fl}^{exp} (the location of the fixed line). This finding suggests that the beam is trapped[30] on the resonance. The jitter in the light blue curves in **b** and **e** is due to the random error of the BPMs ($\sigma_{BPM,x} \approx 0.66$ mm and $\sigma_{BPM,y} \approx 0.5$ mm). The same random error causes the variations in **c**, which make the overlapping trajectory of (Ω, $\bar{a}_y$) appear like a thick ring rather than a circle. The thickness of this ring is consistent with ±3 times the error bar: $\sigma_{\bar{a}_y} \lesssim 2.81$ mm^2 and $\sigma_\Omega \approx 0.0032$, (in units of 2π). In **f**, the dynamic span of $\bar{a}_y$ is much larger than the error bar. Hence, the spiral pattern show resonance trapping.

particle transverse coordinates (x, y) into a resonance phase advance per turn of the form $\Delta\phi_x + 2\Delta\phi_y$, which underlines the possible presence of a nonlinear coupling between the transverse particle coordinates (x, y). When the accelerator tunes are set near this third-order resonance, that is when the distance to this resonance is $\Delta_r = Q_x + 2Q_y - N \approx 0$, the particle dynamics acquires special features due to the nonlinear fields. In particular, the phase advances per turn, $\Delta\phi_x$ and $\Delta\phi_y$, are no longer constant, and the single-particle emittances, ϵ_x and ϵ_y, computed from the particle coordinates as defined by Courant and Snyder[28] are no longer invariant. To emphasize that these quantities vary turn after turn, we call the values of the Courant–Snyder form resulting from the effect of the resonance a_x and a_y (see Methods for their definition). A perturbative approach to the dynamics shows that a_x and a_y must satisfy the relation $2a_x = a_y + C$, where C is a constant determined by the initial conditions. Using only a_y together with the phase advance $\Omega = \phi_x + 2\phi_y$ is sufficient for discussing the properties of the resonance. The key feature of the resonant dynamics for a fixed C is that a pair of values of a_y and Ω exist such that these two dynamical variables become stationary. The theory of fixed lines predicts the existence of an infinite set of these pairs[7]. Back in the four-dimensional phase space (x, p_x, y, p_y), this special solution acquires the topology of a 1D closed curve, i.e. the fixed line[7]. Expressed in Courant–Snyder coordinates, a third-order fixed line is

$$\begin{aligned} \hat{x}(t) &= \sqrt{a_x}\cos(-2t - \alpha + \pi M), \\ \hat{y}(t) &= \sqrt{a_y}\cos(t), \\ \hat{p}_x(t) &= -\sqrt{a_x}\sin(-2t - \alpha + \pi M), \\ \hat{p}_y(t) &= -\sqrt{a_y}\sin(t), \end{aligned} \tag{1}$$

where t is a parameterization variable $0 < t \leq 2\pi$. a_x and a_y are now stationary. α is the resonance driving term angle with respect to the Poincaré surface of section, and the integer M is either 0 or 1 according to the signs of Δ_r and α. From equation (1), we derive the stationary phase advance for a fixed line $\Omega_{fl} = -\alpha + \pi M$, which characterizes its geometric 'orientation' in the phase space.

We report here on the measurement of fixed lines performed at the CERN Super Proton Synchrotron (SPS). Using a set of kicker magnets, we induce transverse oscillations of a proton beam and study how the oscillations are affected by the third-order resonance excited by a few strongly powered sextupoles. The beam positions are measured at each turn using the available beam position monitors (BPMs). With four consecutive BPMs (two per plane), we can reconstruct the Courant–Snyder coordinates $(\hat{x}, \hat{p}_x, \hat{y}, \hat{p}_y)$ at one location of the machine. Taking advantage of the action-angle representation $\hat{x} = \sqrt{a_x}\cos(\phi_x)$, $\hat{p}_x = -\sqrt{a_x}\sin(\phi_x)$, $\hat{y} = \sqrt{a_y}\cos(\phi_y)$ and $\hat{p}_y = -\sqrt{a_y}\sin(\phi_y)$, we can retrieve a_x, a_y, ϕ_x, ϕ_y and Ω (Methods). This procedure allows us to visualize the Poincaré surface of section in Courant–Snyder coordinates and inspect the resonant dynamics in (Ω, a_y) space. If the beam is locked to a stable fixed line, we expect the measured Ω and a_y to be constant, as will be discussed in more detail in the following. A discussion on unstable fixed lines is beyond the scope of this work and may be the subject of future studies.

This experiment faces three major difficulties: (1) The inherent fragility of the effect being searched for. Tune modulation due to a power converter ripple and, therefore, fluctuations of magnetic fields perturb the experimental conditions used to detect fixed lines. To mitigate these effects, we accelerated the beam to 100 GeV/c before exciting transverse beam oscillations, and the machine settings were adjusted carefully (Methods). (2) The intrinsic manufacturing tolerances of accelerator quadrupoles create a well-known effect

https://doi.org/10.1038/s41567-023-02338-3

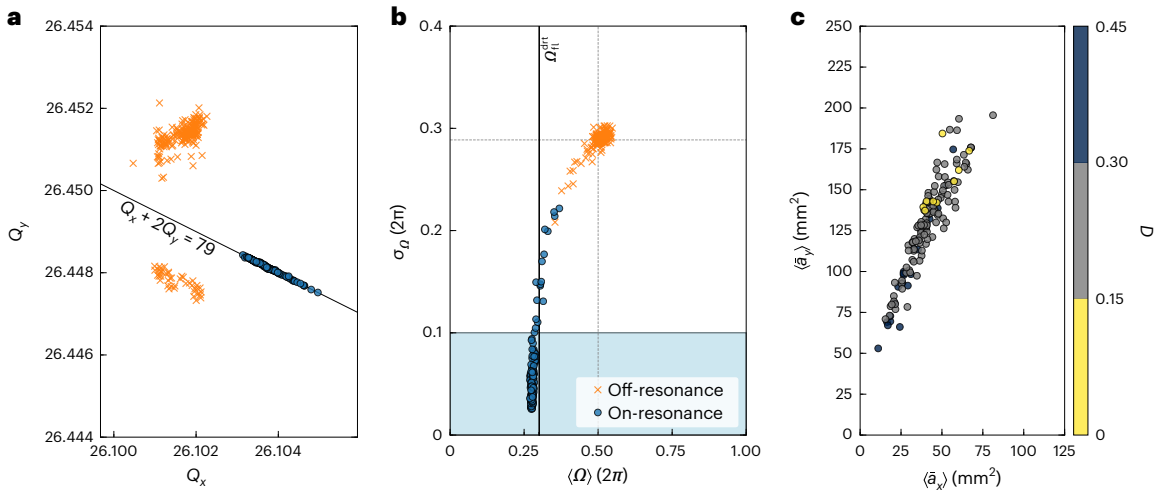

Fig. 4 | Tune diagram, ($\langle\Omega\rangle$, σ_Ω) diagram and ($\langle\bar{a}_x\rangle$, $\langle\bar{a}_y\rangle$) chart. All shots were measured for the same resonance excitation and machine tune settings. **a**, Tune diagram showing the measured average beam tunes along the interval of 3,000 turns. From the total of about 400 shots measured, around 150 shots are on the resonance. The solid line $Q_x + 2Q_y = 79$ is the resonance excited by our sextupole settings. Q_x and Q_y are the betatron tunes, and 79 is the harmonic number of the resonance. The statistical error of tune evaluation is within the marker size. **b**, ($\langle\Omega\rangle$, σ_Ω) diagram. For each shot, we compute the turn-by-turn evolution of Ω along the storage period, and the corresponding mean value $\langle\Omega\rangle$ and standard deviation σ_Ω. The black solid line represents Ω_{fl}^{drt}. The blue area shows the selected shots close to the excited fixed line. Recall that $\Omega = \phi_x + 2\phi_y$ with ϕ_x and ϕ_y the phase advances of the horizontal and vertical planes. Ω_{fl}^{drt} is the resonance phase advance of the resonance we have excited. The dashed lines show what is expected when Ω is not bounded and evolves randomly. In this case, the average of Ω is 0.5, and its standard deviation $\sigma_\Omega = 1/\sqrt{12}$, (in units of 2π). The random error (precision) of $\langle\Omega\rangle$ is $\sigma_{\langle\Omega\rangle} \lesssim 6 \times 10^{-4}$ and, hence, is within the marker size. **c**, Mean values $\langle\bar{a}_x\rangle$ and $\langle\bar{a}_y\rangle$ of the scaled Courant-Snyder forms for the measured shots that are close to the resonance. The quantities $\bar{a}_x$ and $\bar{a}_y$ are the scaled Courant–Snyder forms of the particles. The statistical error bar (precision) of the measured quantities $\langle\bar{a}_x\rangle$ and $\langle\bar{a}_y\rangle$ when the beam is on the fixed line is $\sigma_{\langle\bar{a}_x\rangle} \lesssim 0.5$ mm^2 and $\sigma_{\langle\bar{a}_y\rangle} \lesssim 1.0$ mm^2. In case the beam is not centred on a fixed line, the error bars remain nevertheless within the marker size. The quantity D (Methods and equation (9)), shown by the colour of the markers, indicates the degree of shift in the $\bar{a}_x$ and $\bar{a}_y$ values and, thus, how stable the machine conditions are during the measurement or how close the beam is to the centre of the resonance structure. Small values of D (yellow band) signify that the beam is close to a fixed line and is stationary. If D is large (blue band), then either the beam is far from the fixed line or there has been a drift of the machine parameters (Methods).

called 'beta-beating', which can easily reach a level of the order of ~5%. This unwanted optics perturbation must be considered when analysing measurement results. (3) We must be able to kick the beam onto a fixed line. The SPS has only one vertical and one horizontal kicker suitable for this experiment. This set-up restricts the fixed-line orientations we can explore to the unique value of $\Omega = \Omega_u$ (Methods). In addition, the synchronization of the kickers needs to be taken into account (Methods).

The third-order resonance was excited using two sextupoles placed at proper locations, which enabled us to vary α and, thus, the orientation of the fixed line. To determine the proper sextupole settings, a sequence of measurements was performed by programming the SPS to systematically vary the strength of the two sextupoles, $K_{2,1}$ and $K_{2,2}$, the distance from the resonance Δ_r, and the strength of the horizontal and vertical kicks, θ_x and θ_y, respectively (see Methods for the programming of the SPS).

To analyse the experimental results, we scale the Courant–Snyder coordinates and invariants to $\bar{x}, \bar{p}_x, \bar{y}, \bar{p}_y$, $\bar{a}_x$ and $\bar{a}_y$ (Methods). In Fig. 2, we plot the projections of the measured Poincaré surface of section for 3,000 turns of one selected dataset (all six projections are shown in Extended Data Fig. 1, and Extended Data Fig. 2 shows a comparison with a simulation model). The circular orbits in the horizontal and vertical phase space projections (Fig. 2a,b) show the usual Courant–Snyder invariants, from which we obtain the values of $\bar{a}_x$ and $\bar{a}_y$. The other projections in Fig. 2 exhibit Lissajous patterns. Using these values of $\bar{a}_x$ and $\bar{a}_y$ and applying a least squares minimization, we find the best fit of equation (1) to the experimental data. This curve is shown by the red line in all the projections of Fig. 2. It indicates that the dynamics is consistent with the topology of a fixed line.

From the same dataset, Fig. 3 (top) shows that the distance from the resonance, as obtained from the beam tunes, remains small throughout the storage time (Fig. 3a). $\bar{a}_x$ and $\bar{a}_y$ exhibit only small, correlated oscillations around their corresponding average values (Fig. 3b). The beam revolves around a fixed point in the $(\Omega, \bar{a}_y)$ diagram (Fig. 3c). We determine its orientation to be $\Omega_{fl}^{exp} = 0.275$, (in units of 2π). The line $\Omega_{fl}^{drt} = 0.30$ shows the expected orientation of the fixed line from the sextupole settings[29]. We attribute the difference between Ω_{fl}^{exp} and Ω_{fl}^{drt} to the unavoidable presence of beta-beating. In fact, 5% beta-beating, a value that is pretty normal in hadron accelerators, is sufficient to create a root mean square (r.m.s.) spread in Ω_{fl}^{drt} of 0.016 (Methods), consistent with the experimental findings. The residual beam oscillations around the fixed line in the $(\Omega, \bar{a}_y)$ diagram stems from the experimental inability to move the beam exactly onto the fixed line. For given accelerator optics, there is a unique fixed-line orientation allowed by the location of the kicker magnets (Methods), which for the ideal SPS optics is $\Omega_u = 0.34$. We interpret the difference between the orientation from the ideal lattice Ω_u, the orientation expected from the sextupole driving term Ω_{fl}^{drt} and the orientation determined experimentally Ω_{fl}^{exp} as a result of the combined effect of beta-beating and the granularity of the sextupole scan (see Methods for more details). Note that the turn-by-turn data shown here starts 1,000 turns after the beam is kicked. Particles that are too far away from the stable resonant structure are lost in the machine aperture during the first 1,000 turns (corresponding to around 20 ms storage time), resulting in unreliable readings of the BPMs. This transient has, thus, been excluded in the data analysis presented in this paper.

Figure 3 (bottom) shows a dataset affected by an uncontrolled drift of the SPS machine parameters. In this case, the distance from the resonance exhibits larger variation (Fig. 3d). Nevertheless, although $\bar{a}_x$ and $\bar{a}_y$ decrease over time (Fig. 3e), the beam keeps oscillating around $\Omega_{fl}^{exp} = 0.275$ (Fig. 3f). That is, the resonance is strong enough to trap[30] the beam around the fixed line.

The previous analysis shows that the behaviour of Ω reveals the properties of the resonant dynamics. In particular, the average $\langle\Omega\rangle$ and the standard deviation σ_Ω over the observation period are key quantities for characterizing each beam. Figure 4a shows the measured tunes for a complete set of around 400 different shots (of which around 150 were on the resonance). In this set of measurements, the machine tunes and the sextupoles settings for exciting the third-order resonance were the same as used for the data shown in Fig. 3. Only the strengths of the horizontal and vertical kicks were changed to allow us to probe different amplitudes $\bar{a}_x$ and $\bar{a}_y$. Figure 4b is a $(\langle\Omega\rangle, \sigma_\Omega)$ diagram showing the behaviour of $\langle\Omega\rangle$ for each beam. The shots cluster into two distinct groups: (1) a cluster of off-resonance shots, for which Ω spans all possible angles averaging $\langle\Omega\rangle = 1/2$ with standard deviation $\sigma_\Omega = 1/\sqrt{12}$ and (2) a second cluster close to $\langle\Omega\rangle = \Omega_{\mathrm{fl}}^{\mathrm{drt}}$ with a much lower σ_Ω corresponding to shots where the beam is trapped on the resonance structure. Note that the orientation of all the experimentally found fixed lines is slightly offset compared to the unique orientation, as already observed for the fixed line discussed in the example of Fig. 3. To show more general properties of the fixed lines, we select the shots from Fig. 4b that are closer to $\Omega_{\mathrm{fl}}^{\mathrm{exp}}$ by requiring $\sigma_\Omega < 0.1$ and plot them in the $(\langle\bar{a}_x\rangle, \langle\bar{a}_y\rangle)$ chart in Fig. 4c. The colours of the markers show D, the normalized r.m.s. distance to the fixed line (Methods), arising from drifts of the SPS parameters or from an oscillation around the fixed line. The distribution of the fixed lines in this chart is very similar to what was found in ref. 7.

We have shown that fixed lines may trap beam particles and that we can predict the topology and orientation of the fixed lines, which will allow the development of mitigation strategies to combat beam-degradation mechanisms such as the periodic resonance crossing induced by any modulation of the particle tune or by amplitude-dependent detuning. Our findings are relevant for achieving the high-intensity and high-brightness beams required for both current and future accelerator projects.

Online content

Any methods, additional references, Nature Portfolio reporting summaries, source data, extended data, supplementary information, acknowledgements, peer review information; details of author contributions and competing interests; and statements of data and code availability are available at https://doi.org/10.1038/s41567-023-02338-3.

References

1. Goldstein, H., Poole, C. & Safko, J. *Classical Mechanics* 3rd edn (Addison Wesley, 2002).
2. Goossens, J.-W., Hafermann, H. & Jaouën, Y. Experimental realization of Fermi–Pasta–Ulam–Tsingou recurrence in a long-haul optical fiber transmission system. *Sci. Rep.* **9**, 18467 (2019).
3. Poincaré, H. *Les Méthodes Nouvelles de la Mécanique Céleste*, Vols. 1–3 (Gauthier Villars, 1899).
4. Binney, J. & Tremaine, S. *Galactic Dynamics* 2nd edn (Princeton Univ. Press, 2008).
5. Chao, A. et al. Experimental investigation of nonlinear dynamics in the Fermilab tevatron. *Phys. Rev. Lett.* **61**, 2752–2755 (1988).
6. Schmidt, F. *Untersuchungen zur dynamischen Akzeptanz von Protonenbeschleunigern und ihre Begrenzung durch chaotische Bewegung*. PhD thesis, Hamburg Univ. (1988).
7. Franchetti, G. & Schmidt, F. Extending the nonlinear-beam-dynamics concept of 1D fixed points to 2D fixed lines. *Phys. Rev. Lett.* **114**, 234801 (2015).
8. Chirikov, B. V. A universal instability of many-dimensional oscillator systems. *Phys. Rep.* **52**, 263–379 (1979).
9. Hagedorn, R. *Stability and Amplitude Ranges of Two Dimensional Non-linear Oscillations with Periodical Hamiltonian Applied to Betatron Oscillations in Circular Particle Accelerators* v.1-2. Report No. CERN-1957-001 (CERN, 1957); cds.cern.ch/record/212879
10. Hagedorn, R. & Schoch, A. *Stability and Amplitude Ranges of Two-dimensional Non-linear Oscillations with Periodical Hamiltonian Applied to Betatron Oscillations in Circular Particle Accelerators* v3. Report No. CERN-1957-014 (CERN, 1957); cds.cern.ch/record/213096
11. Schoch, A. *Theory of Linear and Non-linear Perturbations of Betatron Oscillations in Alternating-gradient Synchrotrons*. Report No. CERN-1957-021 (CERN, 1958); cds.cern.ch/record/213137
12. Fischer, W. *An Experimental Study on the Long-term Stability of Particle Motion in Hadron Storage Rings*. PhD thesis, Hamburg Univ. (2005); inspirehep.net/files/212b5649b086be91e38bba97e0a054f7
13. Mais, H., Ripken, G., Wrulich, A. F. & Schmidt, F. *Particle Tracking*. Report No. DESY-86-024 (DESY, 1986); cds.cern.ch/record/166843
14. Chao, A. & Peterson, J. *Status Report SSC Aperture Determination*. Report No. SSC-N-682 (Fermilab, 1988); http://lss.fnal.gov/archive/other/ssc/ssc-n-682.pdf
15. Koutchouk, J.-P. et al. Overview of the LHC dynamic aperture studies. *Conf. Proc. C* **970512**, 1356 (1997); revised version submitted on 19 August 2004.
16. Brüning, O. S. et al. *LHC Design Report*. Report No. CERN-2004-003-V-1 (CERN, 2004); cds.cern.ch/record/782076
17. Maclean, E. H., Tomás, R., Schmidt, F. & Persson, T. H. B. Measurement of nonlinear observables in the Large Hadron Collider using kicked beams. *Phys. Rev. Spec. Top. Accel. Beams* **17**, 081002 (2014).
18. Pellegrini, D. et al. Incoherent beam–beam effects and lifetime optimisation. In *Proc. 8th Evian Workshop on LHC Beam Operation* (eds Dubourg, S., Argyropoulos, T. & Trad, G.) 93–98 (CERN, 2019).
19. Abada, A. et al. FCC-ee: the lepton collider. *Eur. Phys. J. Spec. Top.* **228**, 261–623 (2019).
20. Abada, A. et al. FCC-hh: the hadron collider. *Eur. Phys. J. Spec. Top.* **228**, 755–1107 (2019).
21. Benedikt, M., Blondel, A., Janot, P., Mangano, M. & Zimmermann, F. Future circular colliders succeeding the LHC. *Nat. Phys.* **16**, 402–407 (2020).
22. Spiller, P. & Franchetti, G. The FAIR accelerator project at GSI. *Nucl. Instrum. Methods Phys. Res. A* **561**, 305–309 (2006).
23. Blaurock, J. et al. FAIR completion of construction works, towards commissioning and first science. In *Proc. 14th International Particle Accelerator Conference* (eds Assmann, R. et al.) 3923–3927 (2023).
24. Damerau, H. et al. *LHC Injectors Upgrade, Technical Design Report*. Report No. CERN-ACC-2014-0337 (CERN, 2014); cds.cern.ch/record/1976692
25. Franchetti, G., Hofmann, I., Giovannozzi, M., Martini, M. & Metral, E. Space charge and octupole driven resonance trapping observed at the CERN Proton Synchrotron. *Phys. Rev. Spec. Top. Accel. Beams* **6**, 124201 (2003).
26. Franchetti, G. et al. Experiment on space charge driven nonlinear resonance crossing in an ion synchrotron. *Phys. Rev. Spec. Top. Accel. Beams* **13**, 114203 (2010).
27. Franchetti, G., Gilardoni, S., Huschauer, A., Schmidt, F. & Wasef, R. Space charge effects on the third order coupled resonance. *Phys. Rev. Accel. Beams* **20**, 081006 (2017).
28. Courant, E. & Snyder, H. Theory of the alternating-gradient synchrotron. *Ann. Phys.* **3**, 1–48 (1958).
29. Franchetti, G. Incoherent effects of space charge and sum resonances on particle beams in a storage ring. *Phys. Rev. Accel. Beams* **22**, 114201 (2019).
30. Chao, A. W. & Month, M. Particle trapping during passage through a high-order nonlinear resonance. *Nucl. Instrum. Meth.* **121**, 129–138 (1974).

Methods

Scaled Courant–Snyder coordinates

For an on-momentum particle at fixed energy, the theory of Courant–Snyder defines the normalized dynamical variables as

$$\begin{aligned}\hat{x} &= \frac{1}{\sqrt{\beta_x}}x,\\ \hat{p}_x &= \frac{\alpha_x}{\sqrt{\beta_x}}x + \sqrt{\beta_x}p_x,\\ \hat{y} &= \frac{1}{\sqrt{\beta_y}}y,\\ \hat{p}_y &= \frac{\alpha_y}{\sqrt{\beta_y}}y + \sqrt{\beta_y}p_y,\end{aligned} \tag{2}$$

where x, p_x, y and p_y are the particle phase space coordinates and β_x, α_x, β_y and α_y are the Twiss parameters at the location of the particle[28]. The units of the normalized Courant–Snyder coordinates are $\sqrt{\mathrm{m\,rad}}$. Hence, the Courant–Snyder forms $a_x = \gamma_x x^2 + 2\alpha_x x p_x + \beta_x p_x^2$ and $a_y = \gamma_y y^2 + 2\alpha_y y p_y + \beta_y p_y^2$ have units mrad. In the absence of a resonance, a_x and a_y are the invariants of motion, that is, the particle emittances usually called ϵ_x and ϵ_y. In the presence of a resonance, a_x and a_y can slowly vary. Using these normalized coordinates allows a substantial simplification of the topology of the linear dynamics by making the uncoupled planes of the phase space highly symmetric (linear normal form). The physical beam positions measured by the mth horizonal BPM, the nth vertical BPM and in the direction of the travelling beam by the $(m+1)$th horizontal BPM and the $(n+1)$th vertical BPM are x_m, x_{m+1}, y_n and y_{n+1}, respectively. We will show that by using these measurements we are able to retrieve the Poincaré surface of section.

We start with the observation that the β functions at the locations of all BPMs (in the respective plane of measurement) have almost the same value, which we refer to as $\beta_{\mathrm{BPM}} \approx 103$ m. In the data analysis, we correct the difference in the β functions to β_{BPM}, and define the scaled Courant–Snyder coordinates as

$$\begin{aligned}\bar{x} &= \sqrt{\beta_{\mathrm{BPM}}}\hat{x},\\ \bar{p}_x &= \sqrt{\beta_{\mathrm{BPM}}}\hat{p}_x,\\ \bar{y} &= \sqrt{\beta_{\mathrm{BPM}}}\hat{y},\\ \bar{p}_y &= \sqrt{\beta_{\mathrm{BPM}}}\hat{p}_y,\end{aligned} \tag{3}$$

which have units of metres and automatically imply that a_x and a_y become $\bar{a}_x = \beta_{\mathrm{BPM}} a_x$ and $\bar{a}_y = \beta_{\mathrm{BPM}} a_y$ with units m^2. The phase advance between two consecutive horizontal or vertical BPMs in the SPS is $\pi/2$ within a few percent. In the data analysis, we correct this small shift to restore the phase advance to $\pi/2$. It is thus straightforward to relate these beam position measurements to the scaled coordinates:

$$\begin{aligned}\bar{x}_m &= x_m,\\ \bar{p}_{x,m} &= x_{m+1}\\ \bar{y}_n &= y_n,\\ \bar{p}_{y,n} &= y_{n+1}.\end{aligned} \tag{4}$$

The scaled Courant–Snyder coordinates are, therefore, especially convenient, as they are directly retrieved from the measurement data from two consecutive BPMs.

The sequence of BPMs in the SPS alternates vertical with horizontal position measurements. Therefore, equation (4) needs to be applied with data from a group of four consecutive BPMs, V_n, H_m, V_{n+1} and H_{m+1}. To compute the scaled Poincaré surface of section, we take the location of H_m as our reference position. Although the scaled horizontal phase space is automatically retrieved at the location of H_m, a further rotation of the coordinates $(\bar{y}_n, \bar{p}_{y,n})$ by 40° is necessary to transport the scaled vertical phase space from the location V_n to the location of H_m. This is the treatment of the BPM data necessary to visualize the scaled Poincaré surface of section.

To retrieve the Courant–Snyder coordinates at the location of the horizontal BPM H_m, which is, hence, the Courant–Snyder Poincaré surface of section, we have to invert equations (3) and use the scaled coordinates of the beam. To retrieve the physical coordinates at H_m, namely, to obtain the physical Poincaré surface of section, we need to invert equations (2) using the Twiss parameters at the location H_m and the Courant–Snyder beam coordinates obtained from equations (3).

Constraint on the fixed-line orientation

The possible kick sequence of the two kicker magnets used to deflect the beam from the central orbit has an inherent limitation. In fact, although these two accelerator elements provide two degrees of freedom in displacing the beam in phase space (the kick angles θ_x and θ_y), they are not sufficient to deflect the beam to any point in phase space. This is because with two degrees of freedom, we can access only a 2D surface in the four-dimensional phase space. In fact, the accessible points in the Poincaré surface of section are determined by the optics functions at the location of the kickers and the phase advance to the BPMs.

We consider first the case in which the sequence consists of a vertical kick followed by a horizontal kick. Using equation (1) and solving for t, θ_x and θ_y, which bring the beam onto the fixed line, we find that the only allowed kicks are

$$\theta_x = (-1)^{1+N_\mathrm{k}}\sqrt{\frac{a_x}{\beta_{\mathrm{h},x}}}, \tag{5}$$

$$\theta_y = \pm\sqrt{\frac{a_y}{\beta_{\mathrm{v},y}}}, \tag{6}$$

where $\beta_{\mathrm{h},x}$ is the horizontal beta function at the location of the horizontal kicker, and $\beta_{\mathrm{v},y}$ is the vertical beta function at the location of the vertical kicker, with the integer N_k given by the sign of θ_x. The 'unique orientation' of the fixed line is

$$\Omega_\mathrm{u} = -\alpha + \pi M = 2\Delta\phi_{\mathrm{k},y} - \frac{\pi}{2} + \pi N_\mathrm{k} - \Delta\Omega, \tag{7}$$

where $\Delta\phi_{\mathrm{k},y}$ is the difference between the vertical phase advances of the two kickers.

The quantity $\Delta\Omega$ is defined as $\Delta\Omega = \Omega_\mathrm{h} - \Omega_\mathrm{p}$, with Ω_h the resonance phase at the location of the horizontal kicker and Ω_p the resonance phase at the location of the Poincaré surface of section. $\Delta\Omega$ is computed by counting the phases from the Poincaré surface of section to the kickers. As the horizontal kicker of the SPS can generate only positive deflections, the unique orientation of the fixed line that is consistent with the SPS kicker system is $\Omega_\mathrm{u} = 2\Delta\phi_{\mathrm{k},y} + \pi/2 - \Delta\Omega$ (mod. 2π). Only if the resonance is excited with phase Ω_u and the correct deflecting angles θ_x and θ_y are used can the SPS kicker system shift the beam exactly onto the excited fixed line.

For completeness, we consider also the case in which the kicker sequence is inverted, that is with a horizontal kick followed by a vertical kick. Using the same approach as above, we find the unique fixed-line orientation:

$$\Omega_\mathrm{u} = -\alpha + \pi M = \Delta\phi_{\mathrm{k},x} - \frac{\pi}{2} + \pi N_\mathrm{k} - \Delta\Omega, \tag{8}$$

where we have used the corresponding notation and meaning of quantities as above.

Mitigation of power converter ripple

Increasing the beam energy helps to mitigate the impact of a power converter ripple, as the relative amplitude of the ripple decreases with the higher current required for a higher beam energy.

Kicker synchronization

As the resonance phase at the location of the kickers and the phase advance between the kickers determines the orientation of the fixed line, synchronizing the kickers is critical. During the experimental campaign, the horizontal kicker was fired one turn after the vertical kicker, and therefore, the sequence of beam deflections was vertical followed by horizontal ('Constraint on the fixed-line orientation').

Driving term created by two sextupoles

By knowing the accelerator optics at the location of the BPMs, we can compute the driving term, which has a strength Λ and angle α. By acting on two independent sextupole magnets with strengths $K_{2,1}$ and $K_{2,2}$, respectively, we can easily reach any value of α as long as $\alpha_{K_{2,2}} - \alpha_{K_{2,1}} \approx \pi/2$, where $\alpha_{K_{2,2}}$, and $\alpha_{K_{2,1}}$ denote the angles in the driving term generated by the two sextupoles. During the experimental scan of the sextupole settings, the strength of the driving term was kept constant.

Programming the SPS

The kickers will shift the beam onto a fixed line only if the angle α of the driving term is consistent with the combined effect of both kickers and the accelerator lattice between them. As the SPS has no single sextupole at the proper distance to fulfil this condition, we searched for the fixed lines by scanning the angle α looking for suitable experimental conditions. Once we had an indication of a fixed line, we scanned the distance from the resonance Δ_r and the strength of the resonance, that is the strength of the two sextupoles and the kicker strengths θ_x and θ_y. For each measurement, the beam position was stored turn by turn from all available BPMs in the SPS. Fixed settings for the machine tunes and the resonance excitation were used for the systematic measurements in Fig. 4. These settings were chosen such that a large range of kicker strengths θ_x and θ_y resulted in the trapping of the beam on the resonance structure.

Beam and machine parameters

Optimal experimental conditions were found by setting the SPS to the following parameters: betatron tunes $Q_x = 26.104$ and $Q_y = 26.448$. In addition, the natural chromaticity of the SPS was corrected, i.e. chromaticities are $Q'_x \approx 0$ and $Q'_y \approx 0$, using dedicated sextupole magnets without exciting or notably influencing the third-order resonance. The optimal values of sextupole strengths for exciting the third-order resonance (normalized to the beam rigidity) and kicking the beam onto the fixed line were found to be $K_{2,1} = -0.12\ \mathrm{m}^{-3}$ and $K_{2,2} = -0.21\ \mathrm{m}^{-3}$. In addition, a family of weak octupoles was powered to create some small amplitude-dependent detuning required to stabilize the beam.

The measurements were performed at a plateau of constant beam energy corresponding to a momentum of 100 GeV/c, such that electromagnetic interactions between the particles (collective effects) were negligible compared to the external magnetic guiding fields of the machine. In this case, the beam behaved almost like a single charged particle ('pencil beam'), which made it an ideal probing tool for investigating the nonlinear dynamics of the third-order resonance. A beam with the following characteristics was used: single bunch of 4×10^{10} protons with r.m.s. normalized transverse emittances of $\varepsilon_x \approx 0.5$ µm and $\varepsilon_y \approx 0.5$ µm and a bunch length of about 2.5 ns (4σ). The beam revolution period in the SPS was about 23 µs.

Removing the BPMs noise from $\bar{a}_x$ and $\bar{a}_y$

As the turn-by-turn data suffer from instrumental noise, a 100 turn moving average filter was applied to yield the light blue traces in Fig. 3.

Computing error bars

The values of $\langle \bar{a}_x \rangle$ and $\langle \bar{a}_y \rangle$ are the averages over 3,000 turns after the beam is kicked. The associated error bars are found from the unbiased standard deviation of these data.

The error bars are inferred as follows. From Fig. 2a,b, we see that the distribution of the dots (each dot is a phase space measurement) is confined within a ring. The error introduced by the horizontal BPM is estimated as the thickness of the ring when intercepting the x axis, whose value is $\Delta\bar{x} \approx 4$ mm. In a similar way, from Fig. 2b we find $\Delta\bar{y} \approx 3$ mm. Next, we take this thickness to be six times the standard deviation due to BPM fluctuations. These estimates include ~99% of the fluctuations and are conservative, as in Fig. 2a,b, some additional fluctuations arise because the beam is not exactly centred on the fixed-line structure. Therefore, we take the BPM random errors to be $\sigma_{\mathrm{BPM},x} \approx 4/6 = 0.66$ mm and $\sigma_{\mathrm{BPM},y} \approx 3/6 = 0.5$ mm.

We then use these random errors in an algorithm that repeats the identical procedure for retrieving $\bar{a}$ and ϕ from the BPM measurements, as described for the scaled Courant–Snyder coordinates method. In this algorithm, the beta-beating is also taken into account, as it adds a systematic shift to the beta function and a systematic displacement of the phase advance, thus adding another source of error to the determination of $\bar{a}$ and ϕ. As the actual values of the beta-beating and phase advance shift along the machine are not known with high precision, we calculate the statistics also for these quantities, using the knowledge that the beta-beating in the SPS is $(\delta\beta_x/\beta_x)_{\mathrm{rms}} \approx 5\%$. This procedure allows us to estimate the range of the fluctuations of the quantities we plot in Figs. 3 and 4, for which the estimates for the error bars are mentioned in the relative captions.

Selection of the experimental data and drift parameter

To select the datasets to be analysed, we adopted the same procedure used to verify the data in Fig. 4, namely, by investigating the oscillatory properties in a $(\Omega, \bar{a}_y)$ diagram. The location of the kickers constrains the fixed line to a unique orientation Ω_{u}. However, the granularity of the scan of the sextupole strengths leaves some uncertainty in fulfilling this condition. We, therefore, adopt the standard deviation σ_Ω over the storage time, that is of the oscillation amplitude of Ω, as a measure of closeness to the resonance. We consider a beam to be locked onto a resonance if $\sigma_\Omega \leq 10\%$. When identifying a fixed line, in addition to the locking property, the quantities $\bar{a}_x$ and $\bar{a}_y$ should not suffer from large variations. We measure this effect by defining a parameter D as

$$D = \sqrt{\frac{\sigma^2_{\bar{a}_x}}{\langle \bar{a}_x \rangle^2} + \frac{\sigma^2_{\bar{a}_y}}{\langle \bar{a}_y \rangle^2}}, \tag{9}$$

where $\sigma^2_{\bar{a}_x}$ and $\sigma^2_{\bar{a}_y}$ are the variances of $\bar{a}_x$ and $\bar{a}_y$. Therefore, D corresponds to the normalized r.m.s. distance to the fixed line. Small values of D correspond to cases where the beam is very close to a fixed line with stationary machine parameters (for example $D = 0.11$ in Fig. 3c). On the other hand, a large D means either that the beam is far from the fixed line or that there has been a drift of the machine parameters (for example, $D = 0.36$ in Fig. 3f).

Effect of beta-beating and of the sextupole scan granularity

The effect of beta-beating was estimated by taking the ideal accelerator structure and imparting a tiny random error in the strength of each quadrupole. This perturbed structure was used to compute the driving term angle, hence the associated fixed-line orientation $\Omega_{\mathrm{fl}}^{\mathrm{drt}}$, as well as the perturbed beta functions β_x and β_y. Repeating this procedure enables a statistical analysis. Extensive simulations confirmed that the method of averaging the instantaneous Ω allows $\Omega_{\mathrm{fl}}^{\mathrm{drt}}$ to be retrieved and that $\sigma_{\Omega_{\mathrm{fl}}^{\mathrm{drt}}}/[\sigma_{\beta_y}/\langle\beta_y\rangle] = 3.23 \times 10^{-3}$, where $\sigma_{\Omega_{\mathrm{fl}}^{\mathrm{drt}}}$ is the standard deviation of the set of perturbed $\Omega_{\mathrm{fl}}^{\mathrm{drt}}$, and $\sigma_{\beta_y}/\langle\beta_y\rangle$ is the beta-beating at the location of the sextupoles expressed in percent. Therefore, for a beta-beating of ~5%, we find $\sigma_{\Omega_{\mathrm{fl}}^{\mathrm{drt}}} \approx 0.016$.

The scan of the two sextupoles was carried out while keeping the driving term amplitude constant and varying the two sextupole strengths $K_{2,1}$ and $K_{2,2}$ consistently to change only the phase of the

driving term. Therefore, the maximum error in the orientation of the fixed line $\Omega_{\mathrm{fl}}^{\mathrm{drt}}$ is $\Delta\Omega_{\mathrm{fl}}^{\mathrm{drt}} = 1/(2N)$, with N the number of scan steps in changing the driving term angle. In the experiment, we used $N = 18$. Hence, $\sigma_{\Omega_{\mathrm{fl}}^{\mathrm{drt}}} = (1/18)/(2\sqrt{3}) \simeq 0.016$. This error is comparable with the error for the beta-beating.

Simulation with MAD-X

The experimental conditions are very well defined, and we have a sophisticated tracking model of the ideal SPS lattice in MAD-X format[31], such that one particle is tracked with initial conditions close to the resonance. The results of the simulation are shown in Extended Data Fig. 2a–f. The simulation[32] shows very similar orientations in the six different projections of the Poincaré surface of section as found in the experimental data[33] (Extended Data Fig. 1a–f). The fixed-line orientation for the ideal SPS lattice is $\Omega_{\mathrm{fl}}^{\mathrm{sim}} = 0.290$.

Data availability

The experimental data are available at https://doi.org/10.5281/zenodo.8278600 (ref. 33).

Code availability

Code and simulation analysis are available at https://doi.org/10.5281/zenodo.8266916 (ref. 32).

References

31. De Maria, R., Persson, T., Deniau, L., Schmidt, F. & Grote, H. MethodicalAcceleratorDesign/MAD-X: 5.09.00 (v.5.09.00). *Zenodo* https://doi.org/10.5281/zenodo.7900976 (2023).
32. Bartosik, H., Schmidt, F. & Franchetti, G. Simulation data for SPS fix-line study of a coupled sextupole resonance. *Zenodo* https://doi.org/10.5281/zenodo.8266916 (2023).
33. Bartosik, H., Schmidt, F. & Franchetti, G. SPS fixed line experiment - experimental data [Data set]. *Zenodo* https://doi.org/10.5281/zenodo.8278600 (2023).

Acknowledgements

We would like to acknowledge M. Titze, who contributed to the early experimental investigations in this study. Furthermore, we would like to thank M. Bai, O. Boine Frankenheim, M. Steck and U. Weinrich (GSI), and R. Jones, V. Kain, Y. Papaphilippou and F. Zimmermann (CERN), as well as the operation team at CERN for their support at various stages of this study. The publication is funded by the Deutsche Forschungsgemeinschaft (German Research Foundation) through Grant No. 491382106 and by the Open Access Publishing Fund of GSI Helmholtzzentrum für Schwerionenforschung.

Author contributions

All authors made equal contributions to this work.

Funding

Open access funding provided by GSI Helmholtzzentrum für Schwerionenforschung GmbH.

Competing interests

The authors declare no competing interests.

Additional information

Extended data Extended data are available for this paper at https://doi.org/10.1038/s41567-023-02338-3.

Correspondence and requests for materials should be addressed to H. Bartosik, G. Franchetti or F. Schmidt.

Peer review information *Nature Physics* thanks Giulio Stancari, Jingyu Tang and the other, anonymous, reviewer(s) for their contribution to the peer review of this work.

https://doi.org/10.1038/s41567-023-02338-3

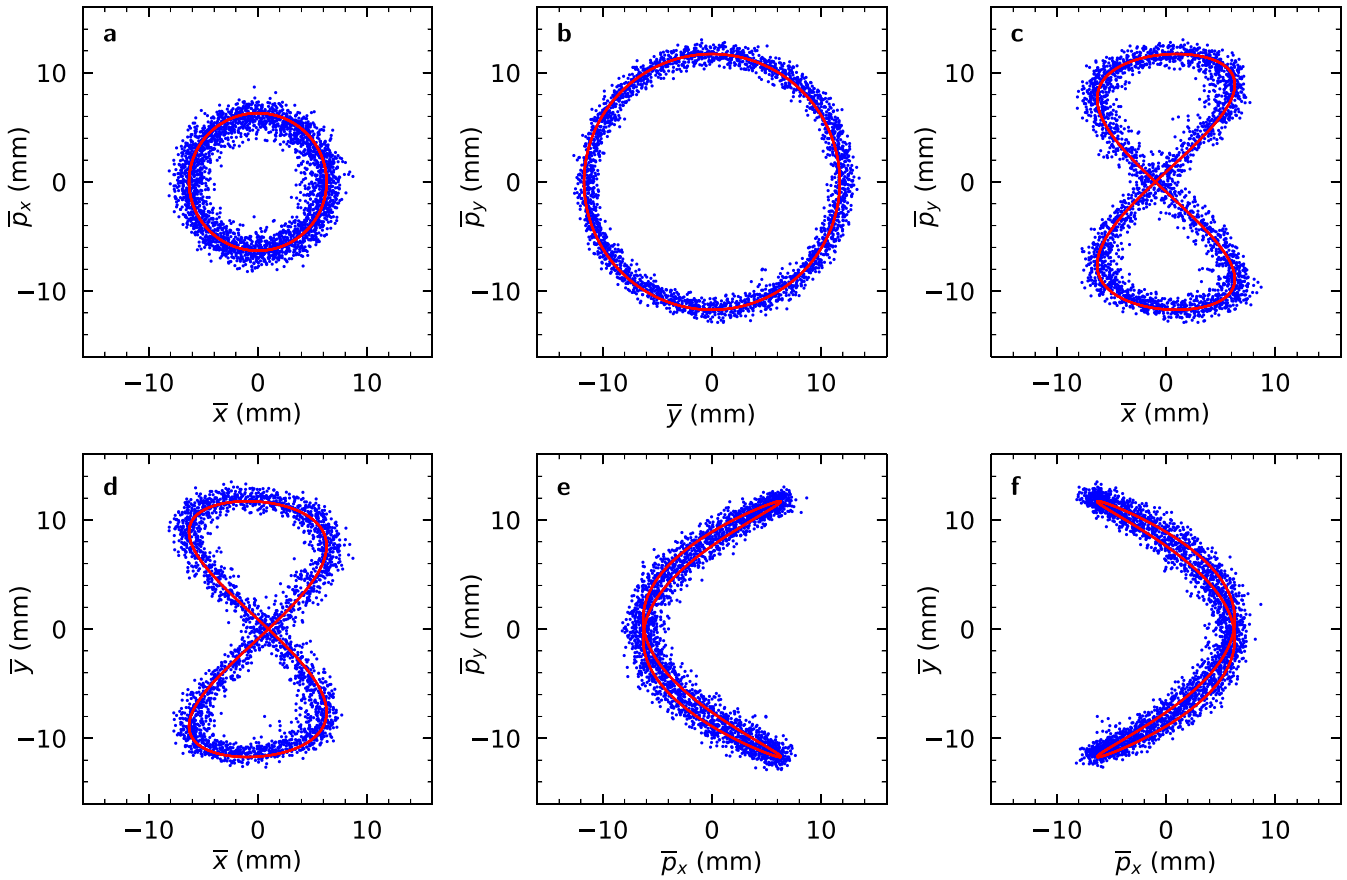

Extended Data Fig. 1 | Full set of projections of a measured Poincaré surface of section. In these pictures (**a**-**f**) we show all 6 two-dimensional phase space projections. The data corresponds to the same shot as shown in Fig. 2. The blue markers are the normalized beam coordinates obtained experimentally from 3,000 passages through the selected longitudinal observation point. The spread of the markers yields a direct information on the random error created by the four BPMs, with a standard deviation $\sigma_{\mathrm{BPM},x} \approx 0.66$ mm, and $\sigma_{\mathrm{BPM},y} \approx 0.5$ mm. The red line is the best fit of Eq. (1) to the experimental data, which confirms that the topology is consistent with a fixed line.

https://doi.org/10.1038/s41567-023-02338-3

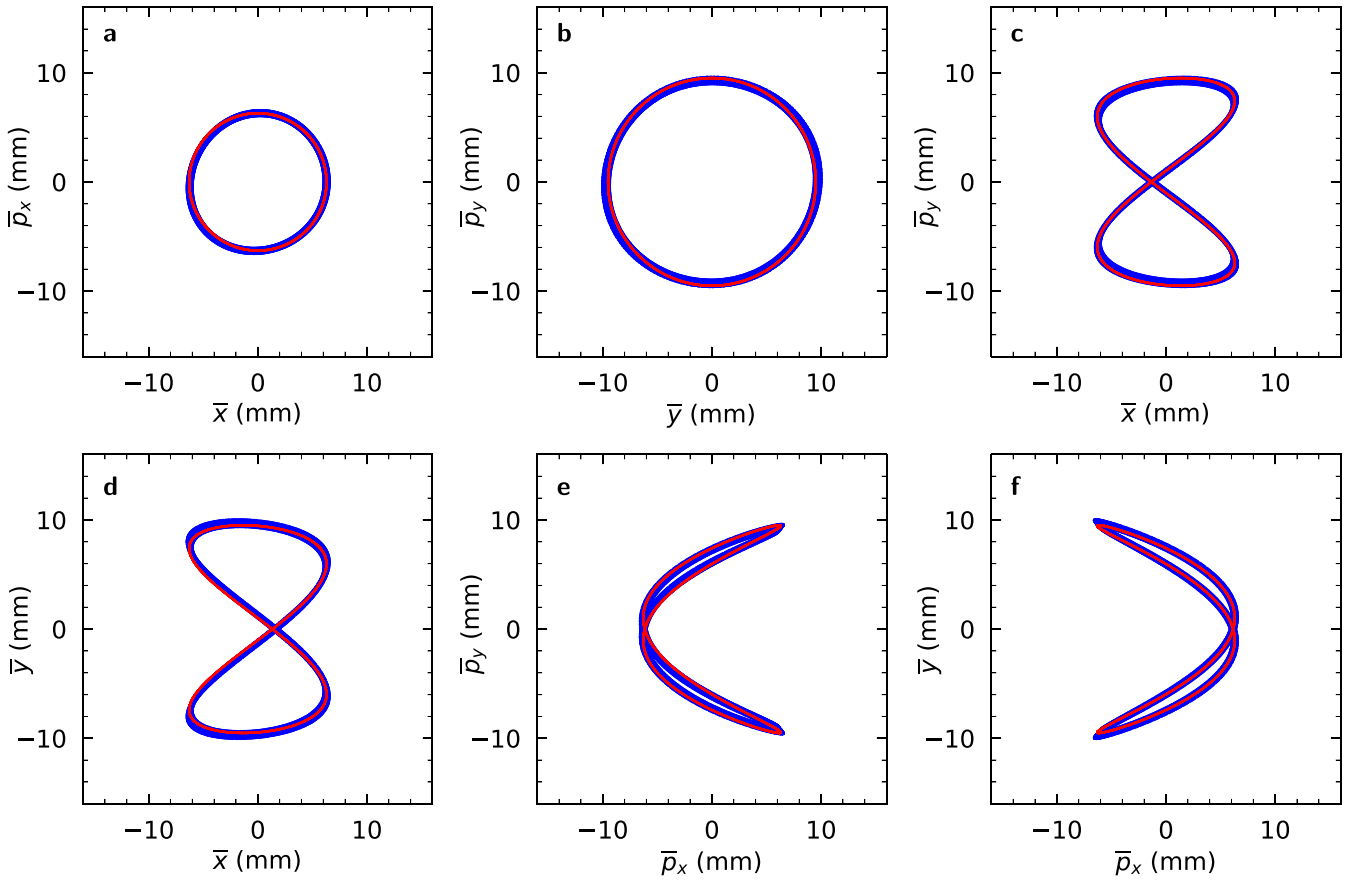

Extended Data Fig. 2 | Simulation model of the SPS. In these pictures (**a**-**f**) we show all 6 two-dimensional phase space projections as obtained from tracking simulations using the MAD-X code[31] with the same sextupole settings as used in the experiment (cf. Extended Data Fig. 1). The red line is the best fit of Eq. (1) to the simulation data. The obtained results are very similar to the experimental data shown in Extended Data Fig. 1, except that in the simulation the starting coordinates were initialized closer to the fixed line and thus reducing the jitter around the fixed line structure. Note that the simulation is not affected by BPM noise.